High-pressure Synthesis and Characterization of the Rare-earth Borate $La_4B_{10}O_{21}$

Ernst Hinteregger, Gunter Heymann, Thomas S. Hofer, and Hubert Huppertz

Institut für Allgemeine, Anorganische und Theoretische Chemie, Leopold-Franzens-Universität Innsbruck, Innrain 80 – 82, 6020 Innsbruck, Austria

Reprint requests to H. Huppertz. E-mail: Hubert.Huppertz@uibk.ac.at

Z. Naturforsch. **2012**, *67b,* 605 – 613 / DOI: 10.5560/ZNB.2012-0001
Received December 9, 2011

Dedicated to Professor Wolfgang Beck on the occasion of his 80th birthday

The lanthanum(III)-decaborate $La_4B_{10}O_{21}$ was synthesized under high-pressure/high-temperature conditions of 2.6 GPa and 750 °C in a Walker-type multianvil apparatus. The single-crystal structure determination revealed that $La_4B_{10}O_{21}$ is isotypic to $Pr_4B_{10}O_{21}$. $La_4B_{10}O_{21}$ crystallizes monoclinically with four formula units in the space group $P2_1/n$ with the lattice parameters a = 716.7(2), b = 1971.5(4), c = 958.3(2) pm, and β = 93.7(1)°. The three-dimensional boron-oxygen framework consists of $[BO_4]^{5-}$ tetrahedra and trigonal-planar $[BO_3]^{3-}$ groups. The structure contains four crystallographically different lanthanum ions. Two of the ions are surrounded by 10, one by 11, and the fourth one by 12 oxygen anions. In addition to IR-spectroscopic investigations, DFT calculations were performed to support the assignment of vibrational bands.

Key words: High Pressure, Borate, Crystal Structure, DFT

Introduction

The system La-B-O is represented by four compositionally different oxoborates with the formulae $LaBO_3$ for λ-$LaBO_3$ [1] and the high-temperature modification H-$LaBO_3$ [2], LaB_3O_6 for one normal pressure oxoborate [3] and two high-pressure modifications, namely γ-LaB_3O_6 [4] and δ-LaB_3O_6 [5], $La_4B_{14}O_{27}$ [6], and $La_{26}O_{27}(BO_3)_8$ [7]. Except for the two high-pressure modifications of the lanthanum-meta-borate γ-LaB_3O_6 and δ-LaB_3O_6, all known lanthanum oxoborates are synthesized by heating of stoichiometric mixtures of La_2O_3 and B_2O_3 under ambient pressure conditions. As a common trend in high-pressure oxoborates, the boron atoms favor the fourfold coordination with increasing pressure. In the majority of cases, the trigonal-planar $[BO_3]^{3-}$ groups transform into tetrahedral $[BO_4]^{5-}$ groups at a pressure higher than 10 GPa. Beyond this threshold, only a few compounds are known which contain trigonal-planar $[BO_3]^{3-}$ groups, *e. g.* $Ho_{31}O_{27}(BO_3)_3(BO_4)_6$ [8]. Additionally, our team observed that these tetrahedra, which are normally linked *via* common corners, can share common edges to realize denser structures [$RE_4B_6O_{15}$ (RE = Dy, Ho) [9 – 11] and α-$RE_2B_4O_9$ (RE = Sm–Ho)] [12 – 14]). Furthermore, under high-pressure conditions the rare-earth ions can show increased coordination numbers (CN), and also the coordination numbers of the oxygen atoms can be enhanced from two-fold coordinated ($O^{[2]}$) to three-fold coordinated ($O^{[3]}$). With the high-pressure/high-temperature synthesis of $La_4B_{10}O_{21}$, we add a new compound to the existing lanthanum-oxoborates. This compound is isotypic to $Pr_4B_{10}O_{21}$ [15]. In the following, we describe the synthesis, the single-crystal structure determination, IR spectroscopic investigations, and quantum-chemical calculations of harmonic vibrational frequencies of $La_4B_{10}O_{21}$.

Experimental Section

Synthesis

The synthesis of $La_4B_{10}O_{21}$ was achieved under high-pressure/high-temperature conditions of 2.6 GPa and 750 °C during experiments to synthesize new lanthanum fluorido- and fluoride borates. For the synthesis, a non-stoichiometric mixture of partially hydrolyzed La_2O_3, LaF_3, and B_2O_3 (all chemicals from Strem Chemicals, Newburyport, USA, 99.9 %) in a molar ratio of 2 : 1 : 6 was finely ground and filled into a boron nitride crucible (Henze BNP GmbH, HeBoSint® S100, Kempten, Germany). The crucible was

placed into an 18/11-assembly and compressed by eight tungsten carbide cubes (TSM-10, Ceratizit, Reutte, Austria). To apply the pressure, a 1000 t multianvil press with a Walker-type module (both devices from the company Voggenreiter, Mainleus, Germany) was used. The assembly and its preparation are described in refs. [16–20]. The mixture of the starting materials was compressed to 2.6 GPa within 1 h and kept at this pressure. During the heating period, the temperature was increased to 750 °C in 10 min, kept there for 10 min, and lowered to 450 °C within 15 min, followed by quenching to r. t. The decompression of the assembly required three hours. The recovered octahedral pressure medium (MgO, Ceramic Substrates & Components Ltd., Newport, Isle of Wight, UK) was broken apart, and the sample was separated from the surrounding boron nitride crucible. The compound $La_4B_{10}O_{21}$ was found in the form of colorless air-stable crystals.

All efforts to synthesize $La_4B_{10}O_{21}$ under ambient pressure conditions were not successful. The high-temperature syntheses were performed in boron nitride crucibles (Henze BNP GmbH, HeBoSint® S100, Kempten, Germany) which were placed into a silica glass tube. This assembly was heated under ambient-pressure conditions in a tube furnace from the company Carbolite.

Crystal structure analysis

The powder diffraction pattern was obtained in transmission geometry, using a Stoe Stadi P powder diffractometer with Ge(111)-monochromatized Mo$K_{\alpha 1}$ (λ = 70.93 pm) radiation. The diffraction pattern showed reflections of $La_4B_{10}O_{21}$ and LaF_3. Fig. 1 shows the experimental powder pattern that matches well with the theoretical pattern simulated from the single-crystal data. Small single crystals of $La_4B_{10}O_{21}$ were isolated by mechanical fragmentation.

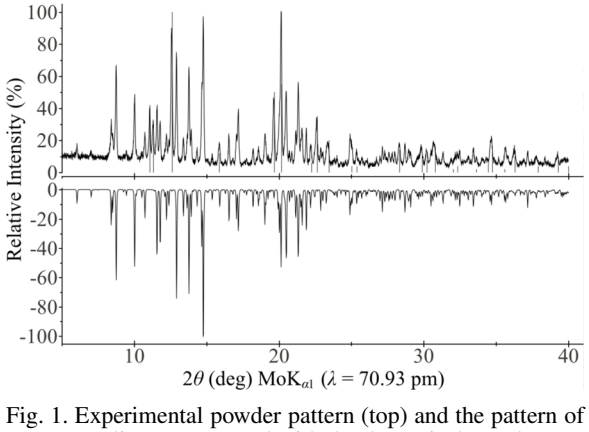

Fig. 1. Experimental powder pattern (top) and the pattern of LaF_3 (top, lines), compared with the theoretical powder pattern of $La_4B_{10}O_{21}$ (bottom), simulated from single-crystal data.

Table 1. Crystal data and structure refinement of $La_4B_{10}O_{21}$ (standard deviations in parentheses).

Empirical formula	$La_4B_{10}O_{21}$
Molar mass, g mol^{-1}	999.74
Crystal system	monoclinic
Space group	$P2_1/n$
Single crystal diffractometer	Enraf-Nonius Kappa CCD
Radiation; wavelength λ, pm	MoK_α; 71.073 (graphite monochromator)
Single-crystal data	
a, pm	716.7(2)
b, pm	1971.5(4)
c, pm	958.3(2)
β, deg	93.7(1)
V, Å^3	1351.4(5)
Formula units per cell, Z	4
Calculated density, g cm^{-3}	4.91
Crystal size, mm^3	$0.045 \times 0.025 \times 0.015$
Temperature, K	293(2)
Absorption coefficient, mm^{-1}	12.5
F(000), e	1784
θ range, deg	2.1 – 32.5
Range in hkl	$-10 < h < 10$, $-29 < k < 29$, $-14 < l < 13$
Total no. of reflections	17750
Independent reflections / R_{int} / R_σ	4898 / 0.0479 / 0.0355
Reflections with $I \geq 2\sigma(I)$	4198
Data / ref. parameters	4898 / 317
Absorption correction	multi-scan [21]
Goodness-of-fit on F_i^2	1.135
Final $R1$ / $wR2$ [$I \geq 2\sigma(I)$]	0.0275 / 0.0532
$R1$ / $wR2$ (all data)	0.0376 / 0.0639
Largest diff. peak / hole, e Å^{-3}	2.01 / −1.24

The single-crystal intensity data were collected at r. t. using a Nonius Kappa-CCD diffractometer with graphite-monochromatized MoK_α radiation (λ = 71.073 pm). A semiempirical absorption correction based on equivalent and redundant intensities (SCALEPACK [21]) was applied to the intensity data. All relevant details of the data collection and evaluation are listed in Table 1. According to the systematic extinctions, the monoclinic space group $P2_1/n$ was derived. Because $La_4B_{10}O_{21}$ is isotypic to $Pr_4B_{10}O_{21}$ [7], the structural refinement was performed *via* the positional parameters of $Pr_4B_{10}O_{21}$ as starting values [SHELXL-97 [22, 23] (full-matrix least-squares on F^2)]. All atoms were refined with anisotropic displacement parameters, and the final difference Fourier syntheses did not reveal any significant peaks in the refinement. Tables 2 – 5 list the positional parameters, anisotropic displacement parameters, and interatomic distances.

Further details of the crystal structure investigation may be obtained from Fachinformationszentrum Karlsruhe, 76344 Eggenstein-Leopoldshafen, Germany (fax: +49-7247-808-666; e-mail: crysdata@fiz-karlsruhe.de, http://www.fiz-karlsruhe.de/request_for_deposited_data.html) on quoting the deposition number CSD-424159.

Table 2. Atomic coordinates (Wyckoff positions 4*e* for all atoms) and equivalent isotropic displacement parameters U_{eq} (Å^2) of $La_4B_{10}O_{21}$ (space group: $P2_1/n$) with standard deviations in parentheses. U_{eq} is defined as one third of the trace of the orthogonalized U_{ij} tensor.

Atom	x	y	z	U_{eq}	Atom	x	y	z	U_{eq}
La1	0.37376(3)	0.20021(2)	0.83910(2)	0.00541(6)	La2	0.89590(3)	0.29516(2)	0.82397(2)	0.00507(6)
La3	0.36452(3)	0.41818(2)	0.84153(2)	0.00488(6)	La4	0.84809(3)	0.07973(2)	0.85067(3)	0.00555(6)
B1	0.0184(6)	0.4068(2)	0.0537(5)	0.0046(8)	B2	0.8092(6)	0.4784(2)	0.8927(5)	0.0050(8)
B3	0.0294(6)	0.4063(2)	0.5544(5)	0.0042(8)	B4	0.2979(6)	0.0247(2)	0.8952(5)	0.0051(8)
B5	0.7035(6)	0.4216(2)	0.6349(5)	0.0042(7)	B6	0.5483(7)	0.3112(2)	0.5462(5)	0.0054(8)
B7	0.7127(7)	0.2053(2)	0.1220(5)	0.0053(8)	B8	0.1971(7)	0.0728(2)	0.6292(5)	0.0056(8)
B9	0.5660(7)	0.3215(2)	0.0473(5)	0.0060(8)	B10	0.6830(6)	0.2012(2)	0.6195(5)	0.0059(8)
O1	0.3026(4)	0.5213(2)	0.9806(3)	0.0057(5)	O2	0.6333(4)	0.1576(2)	0.0183(3)	0.0057(5)
O3	0.3562(6)	0.1180(2)	0.6287(3)	0.0054(5)	O4	0.1300(4)	0.3446(2)	0.0181(3)	0.0054(5)
O5	0.8793(4)	0.3864(2)	0.6392(3)	0.0054(5)	O6	0.0508(4)	0.1776(2)	0.8989(3)	0.0066(5)
O7	0.1704(4)	0.0415(2)	0.7674(3)	0.0059(5)	O8	0.4576(4)	0.0709(2)	0.9131(3)	0.0055(5)
O9	0.5721(5)	0.3121(2)	0.9070(3)	0.0079(6)	O10	0.9604(4)	0.4300(2)	0.9133(3)	0.0066(5)
O11	0.6944(4)	0.1869(2)	0.7568(3)	0.0060(6)	O12	0.2199(4)	0.3176(2)	0.7634(3)	0.0061(6)
O13	0.1363(4)	0.4521(2)	0.1383(3)	0.0060(5)	O14	0.8917(4)	0.2344(2)	0.0806(3)	0.0067(5)
O15	0.3239(4)	0.5398(2)	0.2317(3)	0.0054(5)	O16	0.5450(4)	0.3728(2)	0.6297(3)	0.0065(6)
O17	0.0185(4)	0.1150(2)	0.6008(3)	0.0065(5)	O18	0.6798(4)	0.4694(2)	0.5174(3)	0.0070(6)
O19	0.7269(4)	0.2678(2)	0.5812(3)	0.0073(6)	O20	0.0912(4)	0.2314(2)	0.6393(3)	0.0081(6)
O21	0.1636(4)	0.4525(2)	0.6229(3)	0.0072(6)					

Table 3. Anisotropic displacement parameters of $La_4B_{10}O_{21}$ (space group: $P2_1/n$) with standard deviations in parentheses.

Atom	U_{11}	U_{22}	U_{33}	U_{12}	U_{13}	U_{23}
La1	0.0042(2)	0.0068(2)	0.0053(2)	−0.00008(8)	0.00112(8)	0.00044(8)
La2	0.0042(2)	0.0065(2)	0.0046(2)	0.00028(8)	0.00095(8)	−0.00030(8)
La3	0.0056(2)	0.0046(2)	0.0045(2)	−0.00028(8)	0.00065(8)	−0.00004(8)
La4	0.0054(2)	0.0050(2)	0.0063(2)	−0.00021(8)	0.00063(8)	0.00001(8)
B1	0.004(2)	0.004(2)	0.005(2)	0.001(2)	0.001(2)	0.000(2)
B2	0.006(2)	0.004(2)	0.005(2)	−0.001(2)	−0.001(2)	0.001(2)
B3	0.001(2)	0.004(2)	0.007(2)	−0.003(2)	−0.001(2)	0.002(2)
B4	0.003(2)	0.007(2)	0.006(2)	0.001(2)	0.001(2)	0.002(2)
B5	0.003(2)	0.004(2)	0.005(2)	−0.001(2)	0.000(2)	0.001(2)
B6	0.005(2)	0.006(2)	0.005(2)	−0.000(2)	0.000(2)	−0.000(2)
B7	0.009(2)	0.005(2)	0.002(2)	0.000(2)	0.002(2)	−0.002(2)
B8	0.006(2)	0.006(2)	0.005(2)	0.001(2)	−0.001(2)	0.000(2)
B9	0.004(2)	0.007(2)	0.007(2)	0.001(2)	−0.001(2)	0.000(2)
B10	0.006(2)	0.004(2)	0.008(2)	−0.000(2)	0.000(2)	0.001(2)
O1	0.008(2)	0.005(2)	0.004(2)	0.001(2)	0.003(2)	0.001(2)
O2	0.006(2)	0.007(2)	0.004(2)	0.000(2)	−0.001(2)	−0.002(2)
O3	0.005(2)	0.007(2)	0.005(2)	−0.002(2)	0.001(2)	0.001(2)
O4	0.004(2)	0.006(2)	0.007(2)	0.000(2)	0.001(2)	0.001(2)
O5	0.003(2)	0.006(2)	0.007(2)	0.002(2)	0.001(2)	0.001(2)
O6	0.005(2)	0.009(2)	0.006(2)	−0.001(2)	0.002(2)	−0.002(2)
O7	0.005(2)	0.009(2)	0.004(2)	0.001(2)	0.002(2)	0.000(2)
O8	0.005(2)	0.007(2)	0.004(2)	−0.001(2)	0.000(2)	−0.001(2)
O9	0.009(2)	0.008(2)	0.006(2)	0.000(2)	0.001(2)	0.002(2)
O10	0.007(2)	0.007(2)	0.006(2)	0.001(2)	0.002(2)	0.001(2)
O11	0.006(2)	0.008(2)	0.005(2)	0.001(2)	0.001(2)	0.002(2)
O12	0.006(2)	0.008(2)	0.005(2)	−0.001(2)	0.001(2)	0.001(2)
O13	0.008(2)	0.005(2)	0.004(2)	0.000(2)	0.000(2)	−0.003(2)
O14	0.005(2)	0.007(2)	0.008(2)	0.000(2)	0.002(2)	−0.001(2)
O15	0.006(2)	0.006(2)	0.005(2)	−0.001(2)	0.002(2)	0.000(2)
O16	0.006(2)	0.007(2)	0.007(2)	−0.006(2)	0.002(2)	−0.002(2)
O17	0.004(2)	0.006(2)	0.009(2)	0.004(2)	0.000(2)	0.001(2)
O18	0.009(2)	0.008(2)	0.004(2)	0.001(2)	0.003(2)	0.003(2)
O19	0.007(2)	0.005(2)	0.010(2)	0.001(2)	0.001(2)	−0.001(2)
O20	0.009(2)	0.007(2)	0.008(2)	−0.002(2)	0.001(2)	−0.004(2)
O21	0.007(2)	0.004(2)	0.009(2)	0.002(2)	−0.006(2)	−0.003(2)

Table 4. Interatomic lanthanum-oxygen distances (pm) in $La_4B_{10}O_{21}$ (space group: $P2_1/n$) calculated with the single-crystal lattice parameters (standard deviations in parentheses).

La1–O6	246.1(3)	La2–O12	246.9(3)	La3–O12	233.9(3)	La4–O6	244.2(3)
La1–O11	249.0(3)	La2–O5	252.2(3)	La3–O1a	248.6(3)	La4–O11	252.2(3)
La1–O3	258.5(3)	La2–O9	252.3(3)	La3–O15	252.4(3)	La4–O18a	253.1(3)
La1–O2	259.0(3)	La2–O19	261.0(3)	La3–O21	255.6(3)	La4–O13	253.9(3)
La1–O12	264.4(3)	La2–O4	261.2(3)	La3–O9	262.0(3)	La4–O7	260.4(3)
La1–O9	268.1(3)	La2–O11	263.4(3)	La3–O16	263.3(3)	La4–O15	261.8(3)
La1–O19	268.4(3)	La2–O20	264.4(3)	La3–O7	265.1(3)	La4–O2	276.1(3)
La1–O8	270.4(3)	La2–O6	264.9(3)	La3–O17	273.3(3)	La4–O17	284.4(3)
La1–O20	276.6(3)	La2–O14	273.8(3)	La3–O4	285.6(3)	La4–O8	290.5(3)
La1–O14	280.3(3)	La2–O10	282.2(3)	La3–O10	302.8(3)	La4–O18b	294.2(3)
				La3–O1b	308.2(3)	La4–O21	306.7(3)
						La4–O16	308.8(3)
	∅ 264.1		∅ 262.2		∅ 268.3		∅ 273.9

Table 5. Interatomic boron-oxygen distances (pm) in $La_4B_{10}O_{21}$ (space group: $P2_1/n$) calculated with the single-crystal lattice parameters (standard deviations in parentheses).

B1–O13	144.2(6)	B2–O10	144.8(5)	B3–O5	144.3(5)	B4–O21	146.4(5)
B1–O10	145.6(6)	B2–O13	146.2(5)	B3–O21	145.1(5)	B4–O8	146.4(5)
B1–O3	148.8(5)	B2–O1	149.7(5)	B3–O8	148.7(6)	B4–O18	149.3(5)
B1–O4	151.6(5)	B2–O15	152.1(6)	B3–O2	151.4(5)	B4–O7	151.7(6)
	∅ 147.6		∅ 148.4		∅ 147.4		∅ 148.5
B5–O5	143.7(5)	B6–O6	143.0(6)	B7–O12	142.6(5)	B8–O3	144.7(5)
B5–O18	146.9(5)	B6–O16	145.5(5)	B7–O2	145.8(6)	B8–O1	146.3(5)
B5–O16	148.7(5)	B6–O14	149.1(5)	B7–O14	148.2(5)	B8–O7	148.5(5)
B5–O15	151.1(5)	B6–O19	155.9(6)	B7–O20	153.7(5)	B8–O17	153.6(6)
	∅ 147.6		∅ 148.4		∅ 147.6		∅ 148.3
B9–O9	136.0(6)	B10–O11	134.3(6)				
B9–O20	136.9(6)	B10–O4	136.3(6)				
B9–O17	140.3(5)	B10–O19	140.3(5)				
	∅ 137.7		∅ 137.0				

Vibrational spectra

The FTIR-ATR (*A*ttenuated *T*otal *R*eflection) spectra of single crystals were measured with a Bruker Vertex 70 FT-IR spectrometer (spectral resolution 4 cm^{-1}), equipped with an MCT (*m*ercury *c*admium *t*elluride) detector and attached to a Hyperion 3000 microscope in the spectral range of 600 – 4000 cm^{-1}. As mid-infrared source, a Globar (silicon carbide) rod was used. A frustum-shaped germanium ATR crystal with a tip diameter of 100 μm was pressed on the surface of the borate crystal, which crushed it into small pieces of μm-size. 32 scans of the sample were acquired. A correction for atmospheric influences using the OPUS 6.5 software was performed. A mean refraction index of the sample of 1.6 was assumed for the ATR correction.

DFT calculations

In addition to the experimentally recorded IR spectrum, quantum-chemical computations of harmonic vibrational frequencies were performed using the CRYSTAL 09 program [24 – 26]. An important step of a quantum-mechanical calculation of frequencies is the choice of an adequate basis set. A compromise has to be found balancing computational effort and accuracy of the results. To reduce the computational effort, a basis set with an effective core potential (ECP) for the lanthanum atoms was chosen. The best basis set was found based on geometry optimizations and calculations of harmonic vibrational frequencies of the high-pressure modification δ-LaB_3O_6 [6]. To consider the meta-stability of high-pressure modifications, the cell volume was kept constant during the geometry optimization. Out of these results, a well tested basis set for barium [27] including HAYWSC [28 – 30] for the inner electrons, was modified by adding one electron. All-electron basis sets were employed for boron [31] and oxygen [32]. All calculations were performed with the PBESOL functional [33] for the correlation- and exchange-functionals. The test calculation for δ-LaB_3O_6 using the above settings yielded a deviation less than one percent for the lattice parameters and atom positions. The PBE functional [34] was also tested for δ-LaB_3O_6 and $La_4B_{10}O_{21}$, but poorer results were obtained. The overall computation time for the calculations of harmonic vibrational frequencies of $La_4B_{10}O_{21}$ amounted to four weeks on a node with 16 Opteron dual-core 2.8 GHz processors.

Results and Discussion

Synthetic conditions and reproducibility

All efforts to receive $La_4B_{10}O_{21}$ from a stoichiometric mixture of the pure oxides La_2O_3 and B_2O_3 under normal- and high-pressure conditions were not successful. Obviously, additional LaF_3 in the role

Table 6. List of experiments which were performed to prepare $La_4B_{10}O_{21}$.

Conditions of synthesis							Identified products	
Partially hydrolyzed La_2O_3	La_2O_3	$La(OH)_3$	B_2O_3	LaF_3	T(°C)	p (GPa)	Main products	By-products
0	2	0	5	0	700	2.7	δ-LaB_3O_6	
0	1	0	3	1	1000	2.6	α-LaB_3O_6; LaF_3	
2	0	0	6	1	800	2.6	α-LaB_3O_6; LaF_3	
2	0	0	6	1	800	2.6	α-LaB_3O_6; LaF_3	
2	0	0	6	1	750	2.6	$La_4B_{10}O_{21}$; LaF_3	
0	0	1	2	0	750	2.6	δ-LaB_3O_6	$La_4B_{10}O_{21}$
0	2	0	5	0	750	2.6	δ-LaB_3O_6	λ-$LaBO_3$
0	2	0	5	0	550	2.2	α-LaB_3O_6	
0	2	0	5	0	750	3.0	δ-LaB_3O_6	
1	0	0	1	1	1200	n. p.[a]	α-LaB_3O_6; LaF_3	
1	0	0	4	2	800	n. p.[a]	λ-$LaBO_3$; LaF_3	
1	0	0	1	0	750	n. p.[a]	λ-$LaBO_3$	

[a] n. p. = normal pressure.

of a flux during the synthesis is necessary to yield $La_4B_{10}O_{21}$ as the main product. A detailed schedule of all performed syntheses, including educts, reaction conditions, and products is shown in Table 6. The normal-pressure experiments yielded α-LaB_3O_6 and λ-$LaBO_3$. Under high-pressure/high-temperature conditions, the lanthanum-meta-borates α-LaB_3O_6 and δ-LaB_3O_6 were the main-products while syntheses at higher temperatures led to α-LaB_3O_6. This systematic approach led to the conclusion that the new lanthanum oxoborate $La_4B_{10}O_{21}$ is just synthesizable in a small range of pressure and temperature using LaF_3 as a flux material.

Crystal structure of $La_4B_{10}O_{21}$

The structure of $La_4B_{10}O_{21}$ is composed of trigonal $[BO_3]^{3-}$ and tetrahedral $[BO_4]^{5-}$ groups. Eight of ten crystallographically different boron atoms are coordinated by four oxygen ions. The $[BO_3]^{3-}$ and $[BO_4]^{5-}$ groups are linked to a highly condensed three-dimensional network. Fig. 2 shows the structure along

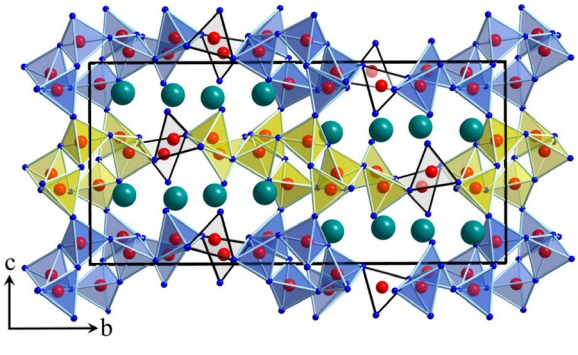

Fig. 2 (color online). Projection of the crystal structure of $La_4B_{10}O_{21}$ along [$\bar{1}$00].

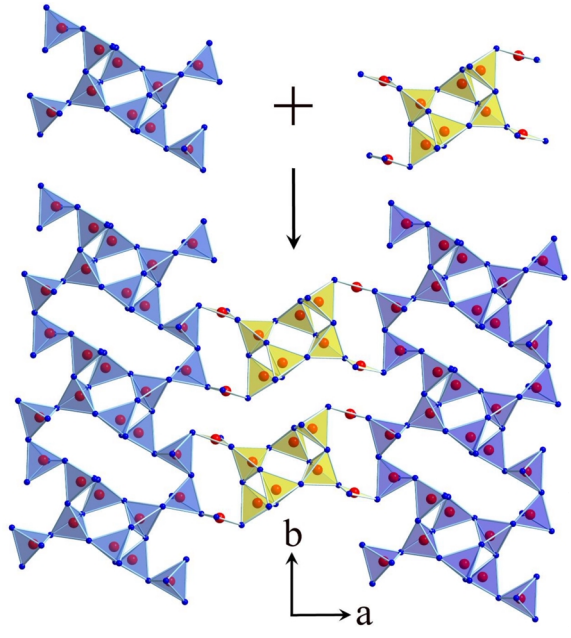

Fig. 3 (color online). Crystal structure of $La_4B_{10}O_{21}$ as viewed along [00$\bar{1}$], showing the boron-oxygen network and the two different building units.

[$\bar{1}$00]. The $[BO_3]^{3-}$ and $[BO_4]^{5-}$ groups form corrugated layers in the *ab* plane, which are marked by differently colored tetrahedra. These layers are linked *via* corner-sharing $[BO_4]^{5-}$ groups. Each layer consists of two different building blocks. The building blocks and their linkage to the layers are illustrated in Fig. 3. The first building block (Fig. 3, top left) consists of ten tetrahedral $[BO_4]^{5-}$ groups. Six tetrahedral groups form a so called central "vierer" ring and two "dreier" rings [35]. On each "dreier" ring, two $[BO_4]^{5-}$ tetrahedra are added. The second building block (Fig. 3, top right) is built up similarly to the first building block

and consists of four trigonal $[BO_3]^{3-}$ and six tetrahedral $[BO_4]^{5-}$ groups. The six tetrahedral groups form the same central "vierer" ring and two "dreier" rings like the first building block. The $[BO_3]^{3-}$ groups substitute the four $[BO_4]^{5-}$ tetrahedra on the outside of the central rings. The two building blocks are linked *via* the outer $[BO_4]^{5-}$ tetrahedra and $[BO_3]^{3-}$ groups.

The boron-oxygen distances inside the eight distinguishable $[BO_4]^{5-}$ groups vary between 142.6(5) (B7–O12) and 155.9(6) pm (B6–O19) with a mean value of 148.0 pm. The trigonal groups show boron-oxygen distances of 136.0(6) – 140.3(5) pm with a mean value of 137.4 pm. The mean values of the boron-oxygen distances correspond well with the known average values for B–O distances in $[BO_4]^{5-}$ and $[BO_3]^{3-}$ groups [36 – 38].

The four crystallographically distinguishable rare-earth cations are located in channels between the layers (Fig. 2). The rare-earth ions La1 and La2 are coordinated by 10 oxygen atoms between 246.1(3) and 280.3(3) pm for La1 and between 246.9(3) and 282.2(3) pm for La2. These values fit well to the La–O distances of α-$La(BO_2)_3$ [d(La–O) = 243 – 285 pm (CN = 10)] [39] and to the tenfold coordinated lanthanum ions in $La_4B_{14}O_{27}$ [d(La–O) = 240.9 – 285.1 pm (CN = 10)] [5]. The third La^{3+} ion (La3) is coordinated by 11 oxygen atoms in the range 233.9(3) – 308.2(3) pm. The fourth lanthanum ion (La4) in $La_4B_{10}O_{21}$ is surrounded by 12 oxygen-atoms with lanthanum-oxygen distances of 244.2(3) – 308.8(3) pm. All distances are listed in the Tables 4 and 5.

The bond-valence sums of $La_4B_{10}O_{21}$ were calculated from the crystal structure for all ions, using the bond-length/bond-strength concept (ΣV) [40, 41]. The calculation revealed values of: +2.93 (La1), +3.23 (La2), +3.06 (La3), and +3.04 (La4) which fit well for the formal ionic charges. For the boron ions, the values vary between 2.95 and 3.04. The oxygen ions show values from −1.86 to −2.24.

Furthermore, the MAPLE values (*MA*delung *P*art of *L*attice *E*nergy) [42 – 44] of $La_4B_{10}O_{21}$ were calculated to compare them with the MAPLE values received from the summation of the binary components La_2O_3 [45] and the high-pressure modification B_2O_3-II [46]. The value of 138125 kJ mol^{-1} was obtained in comparison to 138160 kJ mol^{-1} (deviation = 0.03 %), starting from the binary oxides [La_2O_3 (14234 kJ mol^{-1}) + B_2O_3-II (21938 kJ mol^{-1})].

Table 7. Comparison of the isotypic structures $La_4B_{10}O_{21}$ and $Pr_4B_{10}O_{21}$.

Empirical formula	$La_4B_{10}O_{21}$	$Pr_4B_{10}O_{21}$
Molar mass, g mol^{-1}	999.74	1007.74
Unit cell dimensions		
a, pm	716.7(2)	710.2(2)
b, pm	1971.5(4)	1948.8(4)
c, pm	958.3(2)	951.6(2)
β, deg	93. 7(1)	93.27(3)
V, Å^3	1351.4(2)	1314.9(5)
Coordination number (CN)		
*RE*1 (*RE* = La, Pr)	10	10
*RE*2 (*RE* = La, Pr)	10	10
*RE*3 (*RE* = La, Pr)	11	10
*RE*4 (*RE* = La, Pr)	12	12
av. *RE*1–O (*RE* = La, Pr) distance, pm	264.1	260.7
av. *RE*2–O (*RE* = La, Pr) distance, pm	258.0	258.0
av. *RE*3–O (*RE* = La, Pr) distance, pm	268.3	260.5
av. *RE*4–O (*RE* = La, Pr) distance, pm	273.9	272.1
av. B–O distance in $[BO_3]^{3-}$ groups, pm	137.4	136.8
av. B–O distance in $[BO_4]^{5-}$ groups, pm	148.0	147.5

Despite their isotypy, there is one large difference in the structures of $La_4B_{10}O_{21}$ and $Pr_4B_{10}O_{21}$. Table 7 compares the unit cells, the coordination numbers of the rare-earth metal ions, and the bond lengths. A closer look at the lattice parameters a, b, and c reveals the typical rise due to the higher ionic radius of La^{3+}. The coordination numbers of *RE*1, *RE*2, and *RE*4 (*RE* = La, Pr) are equivalent. In contrast, the coordination number of *RE*3 is different. Fig. 4 shows the relationship between the *RE*–O distances in $La_4B_{10}O_{21}$ and $Pr_4B_{10}O_{21}$. As expected, the *RE*–O distances in $La_4B_{10}O_{21}$ are higher, because of the larger ionic radius of La^{3+}. For *RE*3, the distance to the eleventh oxygen atom differs widely. In contrast to the trend, the oxygen O1b is closer to the metal ion in $La_4B_{10}O_{21}$.

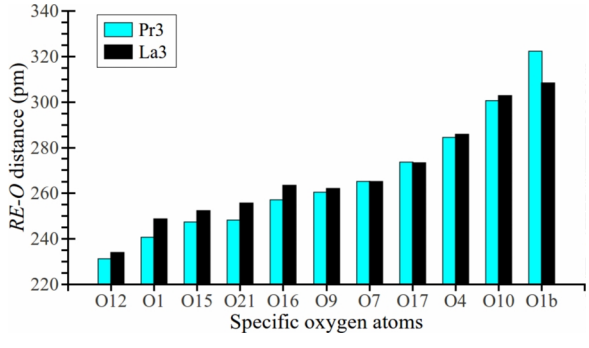

Fig. 4 (color online). *RE*-oxygen distances of Pr3 and La3. Due to the larger ionic radius of La^{3+}, the distances La–O are larger except for the oxygen atom O1b. This deviation yields to a higher coordination number of La3 than Pr3 in $RE_4B_{10}O_{21}$ (*RE* = La, Pr).

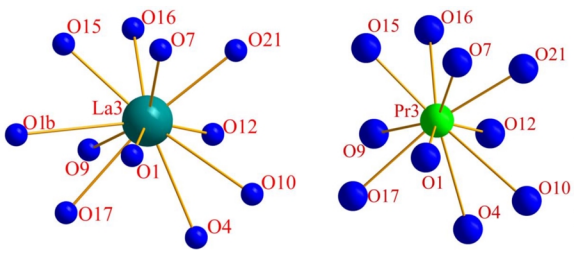

Fig. 5 (color online). Coordination spheres of the *RE*3 ions in $La_4B_{10}O_{21}$ (left) and $Pr_4B_{10}O_{21}$ (right).

Hence, the coordination number of La3 is higher than the coordination number of Pr3. Fig. 5 shows the different coordination spheres of the ions La3 and Pr3.

Vibrational spectroscopy

The spectrum of the FTIR-ATR measurement of $La_4B_{10}O_{21}$ is displayed in Fig. 6. The assignments of the vibrational modes are based on a comparison with the experimental data of borate glasses and crystals, containing trigonal $[BO_3]^{3-}$ and tetrahedral $[BO_4]^{5-}$ groups [47 – 51], and on quantum-mechanical calculations. For borates in general, bands in the region of 800 – 1100 cm^{-1} usually apply to stretching modes of boron which is tetrahedrally coordinated to oxygen atoms [52, 53]. Absorption bands at 1200 – 1450 cm^{-1} are expected for borates containing $[BO_3]^{3-}$ groups [1, 54].

In the FTIR spectrum of $La_4B_{10}O_{21}$, several groups of absorption bands of the boron-oxygen tetrahedra were detected between 680 and 1135 cm^{-1}. The $[BO_3]^{3-}$ modes are found between 1250 and 1450 cm^{-1}. Furthermore, no OH or water bands could be detected in the range of 3000 to 3600 cm^{-1}.

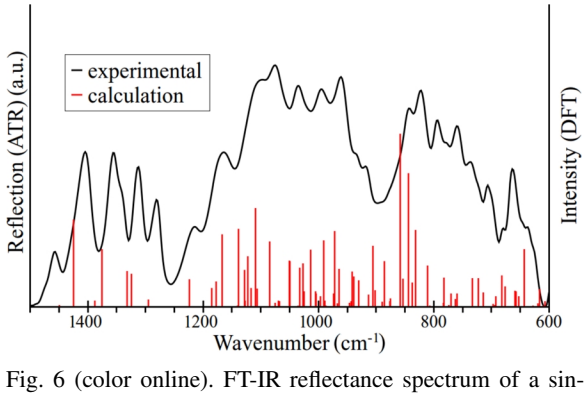

Fig. 6 (color online). FT-IR reflectance spectrum of a single crystal of $La_4B_{10}O_{21}$ (black) and calculated vibrational bands (red lines).

Table 8. Comparison and assignment of theoretical and experimental bands in the spectrum of $La_4B_{10}O_{21}$ [a].

Theoretical band	Experimental band or region	Assignment
1423	1402	$s(B\text{-}O)_{BO_3}, s(O\text{-}B\text{-}O)_{BO_3}$
1374	1352	$s(B\text{-}O)_{BO_3}, s(O\text{-}B\text{-}O)_{BO_3}$
1323	1311	$s(B\text{-}O)_{BO_3}, s(O\text{-}B\text{-}O)_{BO_3}$
1223	1210	$s(O\text{-}B\text{-}O)_{BO_4}, s(O\text{-}B\text{-}O)_{BO_4}, b(B\text{-}O\text{-}B)$
1176	1165	$s(B\text{-}O)_{BO_4}$
1138	1160 – 1110	$s(B\text{-}O)_{BO_4}$
1127	1160 – 1110	$s(B\text{-}O)_{BO_4}, s(O\text{-}B\text{-}O)$
1122	1160 – 1110	$s(B\text{-}O)_{BO_4}$
1108	1160 – 1110	$s(B\text{-}O)_{BO_4}$
1050	1035 – 980	$s(B\text{-}O)_{BO_4}$
1032	1035 – 980	b(O-B-O)
1026	1035 – 980	s(B-O-B)
1024	1035 – 995	$s(B\text{-}O)_{BO_4}$
1012	993	$s(B\text{-}O)_{BO_4}, s(O\text{-}B\text{-}O)$
990	980 – 940	s(O-B-O)
971	980 – 940	$s(B\text{-}O)_{BO_4}$
963	980 – 940	$s(B\text{-}O)_{BO_4}, b(B\text{-}O\text{-}La), b(O\text{-}B\text{-}O)$
941	935 – 925	s(O-B-O)
937	935 – 925	$s(B\text{-}O)_{BO_4}, s(B\text{-}O\text{-}B), b(O\text{-}B\text{-}O)$
905	900 – 885	b(O-B-O)
885	880 – 860	$s(B\text{-}O)_{BO_4}$
857	845	$b(B\text{-}O\text{-}La), b(O\text{-}B\text{-}O), s(B\text{-}O)_{BO_4}$
852	845	$b(B\text{-}O\text{-}La), b(O\text{-}B\text{-}O), s(B\text{-}O)_{BO_4}$
843	825 – 815	s(O-B-O)
837	825 – 815	$s(O\text{-}B\text{-}O), s(B\text{-}O)_{BO_4}$
831	825 – 815	s(B-O-B)
810	792	$b(B\text{-}O\text{-}B), s(B\text{-}O)_{BO_4}$
782	758	b(O-B-O)
732	745 – 695	s(O-B-O)
721	745 – 695	s(B-O-La)
681	665	b(B-O-La), b(O-B-O)

[a] s = stretching; b = bending; in parentheses: pairs of bonded atoms with large relative motion between them; subscript BO_3 and BO_4 refer to the group in which the boron is located.

In the case of $La_4B_{10}O_{21}$, one must consider that all boron-oxygen units are linked to other boron-oxygen units. Hence, every normal mode inside of one boron-oxygen unit induces motions in the connected units. Nevertheless, quantum-chemical calculations (*vide infra*) of harmonic vibrational frequencies could be useful to assign vibrations of excited groups. Fig. 6 shows the experimental IR spectrum in the range of 600 – 1500 cm^{-1} and the calculated modes.

Quantum-mechanical calculations of harmonic vibrational frequencies

Quantum-mechanical calculations of theoretical vibrational modes of large systems like $La_4B_{10}O_{21}$ which contain several heavy atoms like lanthanum are rare. The calculation yields 97 theoretically possible IR-active and 97 Raman-active modes in the

range 600 – 1500 cm^{-1}. Furthermore, the intensities of the IR-active modes were calculated. All calculated vibrational modes show a shift of about 20 cm^{-1} to higher wave numbers. This deviation results out of the approximations in the DFT method, the relatively low convergence for the energy (10^{-7} E_h) and the calculation of just one unit cell. Calculations of larger systems (supercells of $La_4B_{10}O_{21}$) were not possible. Moreover, the calculation did not consider the temperature (297 K for the experiment), and the addition of two Gaussian peaks in the experimental spectrum led to a shift of the maxima.

The large number of theoretical modes prevents a complete assignment of all vibrational modes. The most intensive bands were evaluated, compared with the experimental spectrum and listed in Table 8. In the assignment, the highly condensed boron-oxygen framework must be considered. An exclusive stretching or bending motion inside a building unit is not possible. As expected, in the region of higher wave numbers the excitation happened inside the trigonal $[BO_3]^{3-}$ groups as boron-oxygen stretching. At 1223 cm^{-1} in the calculated spectrum and at 1210 cm^{-1} in the experimental spectrum, the first stretching modes inside of the $[BO_4]^{5-}$ tetrahedra are observed. This is about 100 wave numbers higher than expected for tetrahedral $[BO_4]^{5-}$. Bands at lower wave numbers result from motions of boron and oxygen inside of tetrahedral $[BO_4]^{5-}$ groups. The assignment to $[BO_4]^{5-}$ or $[BO_3]^{3-}$ groups took place to those boron-oxygen units in which the excited bond is located. Bands at lower wave numbers become more and more dominated by bending modes. In the region 940 – 980 cm^{-1} (calculated at 963 cm^{-1}), the first bending mode of a boron-lanthanum-oxygen unit is observed. The first stretching vibrations of the type s(La–O) is located at 721 cm^{-1} in the calculated spectrum.

Conclusions

With the synthesis of $La_4B_{10}O_{21}$, the first isotypic compound to $Pr_4B_{10}O_{21}$ was found and characterized. In accordance with the relatively mild applied pressure of 2.6 GPa, the structure consists of $[BO_4]^{5-}$ tetrahedra and $[BO_3]^{3-}$ groups. 80 % of the boron-oxygen units are represented by BO_4 tetrahedra. The synthesis of the missing isotypic compound in the series $RE_4B_{10}O_{21}$ between lanthanum and praseodymium, $Ce_4B_{10}O_{21}$, will be subject of our future efforts.

Acknowledgements

Special thanks go to Univ.-Prof. Dr. R. Stalder (University of Innsbruck) for performing the IR measurements and Prof. Dr. D. Johrendt (Ludwig-Maximilians University Munich) for the fruitful discussions concerning the DFT calculations. The research was funded by the Austrian Science Fund (FWF): P 23212-N19.

[1] G. K. Abdullaev, G. G. Dzhafarov, Kh. S. Mamedov, *Azerb. Khim. Zh.* **1976**, *1976*, 117.
[2] R. Boelhoff, H. U. Bambauer, W. Hoffmann, *Z. Kristallogr.* **1971**, *133*, 386.
[3] G. K. Abdullaev, Kh. S. Mamedov, G. G. Dzhafarov, *Sov. Phys. Crystallogr.* **1975**, *20*, 161.
[4] H. Emme, C. Despotopoulou, H. Huppertz, *Z. Anorg. Allg. Chem.* **2004**, *630*, 2450.
[5] G. Heymann, T. Soltner, H. Huppertz, *Solid State Sci.* **2006**, *8*, 821.
[6] T. Nikelski, M. C. Schäfer, Th. Schleid, *Z. Anorg. Allg. Chem.* **2008**, *634*, 49.
[7] L. H. Lin, M. Z. Su, K. Wurst, E. Schweda, *J. Solid State Chem.* **1996**, *126*, 287.
[8] S. A. Hering, A. Haberer, R. Kaindl, H. Huppertz, *Solid State Sci.* **2010**, *12*, 1993.
[9] H. Huppertz, S. Altmannshofer, G. Heymann, *J. Solid State Chem.* **2003**, *170*, 320.
[10] H. Emme, H. Huppertz, *Acta Crystallogr. C* **2005**, *61*, i23.
[11] H. Emme, M. Valldor, R. Pöttgen, H. Huppertz, *Chem. Mater.* **2005**, *17*, 2707.
[12] H. Emme, H. Huppertz, *Z. Anorg. Allg. Chem.* **2002**, *628*, 2165.
[13] H. Emme, H. Huppertz, *Chem. Eur. J.* **2003**, *9*, 3623.
[14] H. Emme, H. Huppertz, *Acta Crystallogr. C* **2005**, *61*, i29.
[15] A. Haberer, G. Heymann, H. Huppertz, *J. Solid State Chem.* **2007**, *180*, 1595.
[16] N. Kawai, S. Endo, *Rev. Sci. Instrum.* **1970**, *8*, 1178.
[17] D. Walker, M. A. Carpenter, C. M. Hitch, *Am. Mineral.* **1990**, *75*, 1020.
[18] D. Walker, *Am. Mineral.* **1991**, *76*, 1092.
[19] D. C. Rubie, *Phase Transitions* **1999**, *68*, 431.
[20] H. Huppertz, *Z. Kristallogr.* **2004**, *219*, 330.
[21] Z. Otwinowski, W. Minor in *Methods in Enzymology*, Vol. 276, *Macromolecular Crystallography*, Part A (Eds.: C. W. Carter Jr., R. M. Sweet), Academic Press, New York, **1997**, pp. 307.
[22] G. M. Sheldrick, SHELXL-97, Program for the Refine-

ment of Crystal Structures, University of Göttingen, Göttingen (Germany) **1997**.
[23] G. M. Sheldrick, *Acta Crystallogr.* **2008**, *A46*, 112.
[24] R. Dovesi, V. R. Saunders, C. Roetti, R. Orlando, C. M. Zicovich-Wilson, E. Pascale, B. Civalleri, K. Doll, N. M. I. J. Bush, Ph. D'Arco, M. Llunell, CRYSTAL09-User's Manual, University of Torino, Torino (Italy) **2009**.
[25] R. Dovesi, R. Orlando, B. Civalleri, R. Roetti, V. R. Saunders, C. M. Zicovich-Wilson, *Z. Kristallogr.* **2005**, *220*, 571.
[26] F. Pascale, C. M. Zicovich-Wilson, F. Lopez, B. Civalleri, R. Orlando, R. Dovesi, *J. Comput. Chem.* **2004**, *25*, 888.
[27] S. Piskunov, E. Heifets, R. I. Eglitis, G. Borstel, *Comp. Mat. Sci.* **2004**, *29*, 165.
[28] P. J. Hay, W. R. Wadt, *J. Chem. Phys.* **1984**, *82*, 270.
[29] P. J. Hay, W. R. Wadt, *J. Chem. Phys.* **1984**, *82*, 284.
[30] P. J. Hay, W. R. Wadt, *J. Chem. Phys.* **1984**, *82*, 299.
[31] R. Orlando, R. Dovesi, C. Roetti, *J. Phys.: Condens. Matter.* **1990**, *38*, 7769.
[32] L. Valenzano, F. J. Torres, K. Doll, F. Pascale, C. M. Zicovich-Wilson, R. Dovesi, *Z. Phys. Chem.* **2006**, *220*, 893.
[33] J. P. Perdew, A. Ruzsinszky, G. I. Csonka, O. A. Vydrov, G. E. Scuseria, L. A. Constantin, X. Zhou, K. Burke, *Phys. Rev. Lett.* **2008**, *100*, 136406.
[34] J. P. Perdew, K. Burke, M. Ernzerhof, *Phys. Rev. Lett.* **1996**, *77*, 3865.
[35] The naming of rings of structural elements was coined by F. Liebau (F. Liebau, Structural Chemistry of Silicates, Springer, Berlin, **1985**) and is derived from German numbers, *e. g.* the terms "dreier" rings and "vierer" rings are derived from the words "drei" respectively "vier", which mean three and four. However, the terms "dreier" ring and "vierer" ring do not mean a three-membered or four-membered ring, but rather a ring with three or four tetrahedral centers (B) and three or four electronegative atoms (O).
[36] E. Zobetz, *Z. Kristallogr.* **1990**, *191*, 45.
[37] F. C. Hawthorne, P. C. Burns, J. D. Grice in *Boron: Mineralogy, Petrology and Geochemistry*, (Ed.: E. S. Grew), Mineralogical Society of America, Washington, **1996**.
[38] E. Zobetz, *Z. Kristallogr.* **1982**, *160*, 81.
[39] G. K. Abdullaev, G. G. Dzhafarov, Kh. S. Mamedov, *Sov. Phys. – Crystallogr.* **1981**, *26*, 473.
[40] I. D. Brown, D. Altermatt, *Acta Crystallogr.* **1985**, *B41*, 244.
[41] N. E. Brese, M. O'Keeffe, *Acta Crystallogr.* **1991**, *B47*, 192.
[42] R. Hoppe, *Angew. Chem.* **1966**, *78*, 52; *Angew. Chem., Int. Ed. Engl.* **1966**, *5*, 95.
[43] R. Hoppe, *Angew. Chem.* **1970**, *82*, 7; *Angew. Chem., Int. Ed. Engl.* **1970**, *9*, 25.
[44] R. Hübenthal, M. Serafin, R. Hoppe, MAPLE (version 4.0), Program for the Calculation of Distances, Angles, Effective Coordination Numbers, Coordination Spheres, and Lattice Energies, University of Gießen, Gießen (Germany) **1993**
[45] N. Hirosaki, S. Ogata, C. Kocer, *J. Alloys. Compd.* **2003**, *351*, 21.
[46] C. T. Prewitt, R. D. Shannon, *Acta Crystallogr.* **1968**, *B24*, 869.
[47] H. Huppertz, *J. Solid State Chem.* **2004**, *177*, 3700.
[48] G. Chadeyron, M. El-Ghozzi, R. Mahiou, A. Arbus, J. C. Cousseins, *J. Solid State Chem.* **1997**, *128*, 261.
[49] L. Jun, X. Shuping, G. Shiyang, *Spectrochim. Acta* **1995**, *A51*, 519.
[50] G. Padmaja, P. Kistaiah, *J. Phys. Chem.* **2009**, *A113*, 2397.
[51] J. C. Zhang, Y. H. Wang, X. Guo, *J. Lumin.* **2007**, *122-123*, 980.
[52] M. Ren, J. H. Lin, Y. Dong, L. Q. Yang, M. Z. Su, L. P. You, *Chem. Mater.* **1999**, *11*, 1576.
[53] J. P. Laperches, P. Tarte, *Spectrochim. Acta* **1966**, *22*, 1201.
[54] W. C. Steele, J. C. Decius, *J. Chem. Phys.* **1956**, *25*, 1184.